

Structure, magnetism and magnetocaloric effects in $Er_5Si_3B_x$ ($_x$ = 0.3,0.6) compounds

Zhihong Hao(郝志红), Hui Liu(刘辉), and Juguo Zhang(张聚国)
Citation: Chin. Phys. B, 2023, 32 (**11**): 117501. DOI: 10.1088/1674-1056/ace684
Journal homepage: http://cpb.iphy.ac.cn; http://iopscience.iop.org/cpb

What follows is a list of articles you may be interested in

Effect of TbF_3 diffusion on the demagnetization behavior and domain evolution of sintered Nd-Fe-B magnets by electrophoretic deposition

Xue-Jing Cao(曹学静), Shuai Guo(郭帅), Yu-Heng Xie(谢宇恒), Lei Jin(金磊), Guang-Fei Ding(丁广飞),Bo Zheng(郑波), Ren-Jie Chen(陈仁杰), and A-Ru Yan(闫阿儒)
Chin. Phys. B, 2023, 32 (**9**): 097503. DOI: 10.1088/1674-1056/acaf2d

Magnetic and electronic properties of bulk and two-dimensional $FeBi_2Te_4$: A first-principles study

Qianqian Wang(王倩倩), Jianzhou Zhao(赵建洲), Weikang Wu(吴维康), Yinning Zhou(周胤宁), Qile Li, Mark T. Edmonds, and Shengyuan A. Yang(杨声远)
Chin. Phys. B, 2023, 32 (**8**): 087506. DOI: 10.1088/1674-1056/acd522

Hysteresis loss free soft magnetic ferrites based on Larmor precession

Shuang-Jiu Feng(冯双久), Xin-Li Zhao(赵幸丽), Shou-Jin Zhu(朱守金),Qing-Rong Lv(吕庆荣), Xu-Cai Kan(阚绪材), and Xian-Song Liu(刘先松)
Chin. Phys. B, 2023, 32 (**8**): 087503. DOI: 10.1088/1674-1056/acbdec

Spin reorientation in easy-plane kagome ferromagnet $Li_9Cr_3(P_2O_7)_3(PO_4)_2$

Yuanhao Dong(董元浩), Ying Fu(付盈), Yixuan Liu(刘以轩), Zhanyang Hao(郝占阳), Le Wang(王乐), Cai Liu(刘才), Ke Deng(邓可), and Jiawei Mei(梅佳伟)
Chin. Phys. B, 2023, 32 (**5**): 057506. DOI: 10.1088/1674-1056/acc2b3

Topological magnetotransport and electrical switching of sputtered antiferromagnetic $Ir_{20}Mn_{80}$

Danrong Xiong(熊丹荣), Yuhao Jiang(蒋宇昊), Daoqian Zhu(朱道乾), Ao Du(杜奥), Zongxia Guo(郭宗夏), Shiyang Lu(卢世阳), Chunxu Wang(王春旭), Qingtao Xia(夏清涛), Dapeng Zhu(朱大鹏), and Weisheng Zhao(赵巍胜)
Chin. Phys. B, 2023, 32 (**5**): 057501. DOI: 10.1088/1674-1056/acb9ec

---

Structure, magnetism and magnetocaloric effects in $Er_5Si_3B_x$ ($x = 0.3, 0.6$) compounds

Zhihong Hao(郝志红)[1,†], Hui Liu(刘辉)[2], and Juguo Zhang(张聚国)[3]

[1] *School of Rare Earth and New Materials Engineering, Gannan University of Science and Technology, Ganzhou* 341000, *China*

[2] *School of Intelligent Manufacturing and Automotive Engineering, Gannan University of Science and Technology, Ganzhou Innovation Center of Rare earth Permanent Magnet Material Advanced Manufacturing and Intelligent Equipment Technology, Ganzhou* 341000, *China*

[3] *School of Rare Earth and New Materials Engineering, Gannan University of Science and Technology, Ganzhou Key Laboratory of Advanced Processing and Technology Optimization of High Performance Tungsten Base Materials, Ganzhou* 341000, *China*

(Received 26 May 2023; revised manuscript received 3 July 2023; accepted manuscript online 12 July 2023)

We investigate the structure, magnetic properties, magnetic phase transitions and magnetocaloric effects (MCEs) of $Er_5Si_3B_x$ ($x = 0.3$, 0.6) compounds. The $Er_5Si_3B_x$ ($x = 0.3$, 0.6) compounds crystalize in a Mn_5Si_3 type hexagonal structure (space group: $P63/cm$) and exhibit a successive complicated magnetic phase transition. The extensive magnetic phase transitions contribute to the broad temperature range of MCEs exhibiting in $Er_5Si_3B_x$ ($x = 0.3$, 0.6) compounds, with maximum magnetic entropy change ($-\Delta S_M^{max}$) and refrigeration capacity of 10.2 J·kg^{-1}·K^{-1}, 356.3 J/kg and 11.5 J·kg^{-1}·K^{-1}, 393.3 J/kg under varying magnetic fields 0–5 T, respectively. Remarkably, the δT_{FWHM} values (the temperature range corresponding to $\frac{1}{2} \times |-\Delta S_M^{max}|$) of $Er_5Si_3B_x$ ($x = 0.3$, 0.6) compounds were up to 41.8 K and 39.6 K, respectively. Thus, the present work provides a potential magnetic refrigeration material with a broad temperature range MCEs for applications in cryogenic magnetic refrigerators.

Keywords: magnetic materials, cryogenic magnetic refrigeration, magnetic phase transition, magnetocaloric effects

PACS: 75.30.Sg, 75.47.Np **DOI:** 10.1088/1674-1056/ace684

1. Introduction

Magnetic materials have gained great interest due to their attractive properties and wide applications.[1–7] The novel solid-state refrigeration technology based on the magnetocaloric effect (MCE) is one of the most promising replacements for conventional refrigeration technologies because of its high efficiency and non-emission of pollutants.[8–23] The MCE is the thermodynamic response of the magnetic material to an applied magnetic field, meaning that the magnetic moment transforms from ordered to disordered (or ordered to ordered) during the imposition of an applied magnetic field, resulting in a change in magnetic entropy.[24] The maximum magnetic entropy changes ($-\Delta S_M^{max}$) generally appear near the magnetic phase transition temperature, so the magnetic phase transition is strongly correlated with the MCE.[25] The $-\Delta S_M^{max}$ and the refrigeration capacity (RC) are important indicators of the MCE of magnetic refrigeration materials. It is worth noting that the refrigeration region required for cryogenic magnetic refrigeration technology is within 10–77 K.[26] Therefore, it is imperative to develop magnetic refrigeration materials with wide temperature span MCEs for practical applications.

The search for magnetic refrigeration materials with wide temperature span MCE has involved considerable attempts and efforts. The amorphous materials have a wider range of magnetic transition temperature regions owing to the lack of long-range ordering and as a result have a larger δT_{FWHM} of the $-\Delta S_M$. It has been reported extensively that the MCE with large δT_{FWHM} in amorphous ribbons.[27–30] In addition, the design and development of compounds with different alloy phases with multiple magnetic phase transitions are also considered to be an effective pathway to obtain magnetic refrigeration materials with a wide refrigeration region, such as double-phase $ErZn_2$/ErZn composite and $Ho_{36}Co_{48}Al_{16}$ alloy.[31,32] Meanwhile, materials with a successive magnetic phase transitions are another powerful approach to increasing the refrigeration range. Zhang *et al.* reported that the Ho_3Al_2 compound has δT_{FWHM} up to 47 K owing to the existence of spin reorientation (SR) transitions and ferromagnetic (FM)-to-paramagnetic (PM) transitions.[33] However, the available magnetic refrigeration materials remain gaps in performance for applications, where further improvements in δT_{FWHM} are still an unresolved challenge.

Semitelou *et al.* investigated the magnetic structure of the Er_5Si_3 compound in the temperature range 1.8–120 K by neutron-diffraction measurements.[34] The results show a complex magnetic structure in the Er_5Si_3 compound with two different AFM interactions for wave vectors $K_1 = [0, \pm 1/4, 0]$ and $K_2 = [0, 0, \pm 0.227(2)]$ at 1.8–13 K and 10–29 K, respectively. More surprisingly, the magnetic interaction of the Er_5Si_3 compound in the temperature range 10–13 K coexists with AFM interaction, and a magnetic phase transition

†Corresponding author. E-mail: love_hzh@126.com

© 2023 Chinese Physical Society and IOP Publishing Ltd

from AFM to paramagnetic occurs at 29 K. The Er_5Si_3 compound with multiple successive magnetic phase transitions is an ideal system for investigating the correlation between magnetic phase transitions and MCEs. Furthermore, addition of the interstitial atom element B modulates the orbital exchange interaction of the rare earth ions for the objective of regulating the magnetic ground state.[35] In this work, the structure, magnetic properties, magnetic phase transitions and magnetocaloric properties of $Er_5Si_3B_x$ ($x = 0.3$, 0.6) compounds are studied. The δT_{FWHM} values of $Er_5Si_3B_x$ ($x = 0.3$, 0.6) compounds are up to 41.8 K and 39.6 K under varying magnetic fields from 0 to 5 T, respectively.

2. Experimental

The polycrystalline samples were synthesized by melting the elements Er (purity: 99.9%), Si (purity: 99.9%) and B (purity: 99.9%) ratios on a water-cooled copper bed in a high purity argon atmosphere. The ingots were repeatedly melted four times and overturned after each melting to ensure homogeneity of the sample. Powder x-ray diffraction (XRD) is measured at room temperature using Cu K_α radiation. Based on a quantum design physical properties measurement system (PPMS-9), the measurements of magnetization of the sample was measured by a superconducting quantum interferometer (SQUID) magnetometer and a vibrating sample magnetometer (VSM).

3. Results and discussions

Figures 1(a) and 1(b) show the room-temperature XRD pattern of $Er_5Si_3B_x$ compounds experimentally obtained with Rietica software refinement. The Mn_5Si_3-type hexagonal structure (space group: $P63/mcm$) is adopted to fit the diffraction peaks very well. The parameters of refined and other information about the crystal structure are listed in Table 1. The schematic crystal structure of $Er_5Si_3B_x$ compounds are illustrated in Figs. 1(c) and 1(d). There are two inequivalent Er atoms in $Er_5Si_3B_x$ compounds. The Er atom at the first site is located at the Wyckoff positions 6*g* (0, 0.759, 3/4) and the

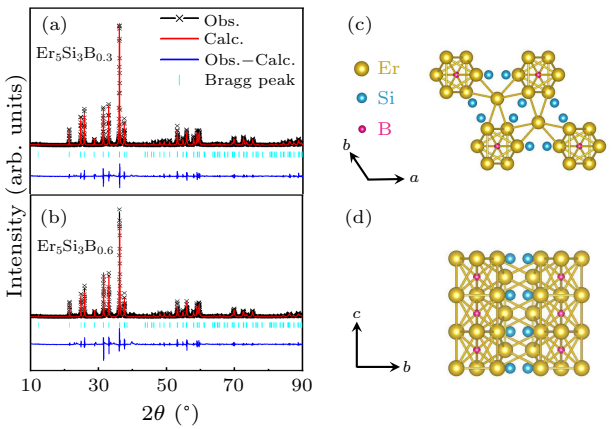


Fig. 1. [(a), (b)] Room-temperature XRD patterns and [(c), (d)] the crystal structure of $Er_5Si_3B_x$ ($x = 0.3$, 0.6) compounds.

Table 1. Rietveld refinement parameters of $Er_5Si_3B_x$ ($x = 0.3$, 0.6) compounds.

Compounds	$Er_5Si_3B_{0.3}$	$Er_5Si_3B_{0.6}$
Space group	Mn_5Si_3-type $P6_3/mcm$ (No. 193)	
a (Å)	8.294	8.289
b (Å)	8.294	8.289
c (Å)	6.205	6.200
V (Å^3)	369.658	368.921
Er	Wyckoff positions 4*d*, 6*g*	
x	2/3, 0	
y	1/3, 0.759	
z	1/2, 3/4	
Si	Wyckoff positions 6*g*	
x	0	
y	0.398	
z	3/4	
B	Wyckoff positions 2*b*	
x	0	
y	0	
z	1/2	
R_p (%)	7.364	8.377
R_{wp} (%)	10.274	12.437
R_F (%)	3.133	4.620

six 6*g* positions of the Er atoms form an octahedral structure. The B atom is located in the center of the octahedron with the corresponding Wyckoff position 2*b* (0, 0, 1/2). The Er atom in the second site is located at Wyckoff position 4*d* (2/3, 1/3, 1/2) and coordinates with the six surrounding equivalent Si atoms located at Wyckoff positions 6*g* (0, 0.398, 3/4). The doping of B element lead to a distention of the *a* and *b* axis of $Er_5Si_3B_x$ compounds compared to the Er_5Si_3 compound, while the *c* axis shows a shorter length. The variation of the lattice constant will cause a dramatic change of the orbital exchange between the elements in the system, which will exhibit complex and fascinating magnetic properties.[36]

In order to understand the magnetic and magnetic phase transitions, the temperature-dependent magnetization curves $M(T)$ for $Er_5Si_3B_x$ compounds were obtained by using field cooling (FC) and zero-field cooling (ZFC) modes, and the corresponding results are shown in Figs. 2(a) and 2(b). The results show that magnetization *M* increases gradually with decreasing temperature, peaks around 30 K, and decreases briefly before rising sharply again. These indicate that the PM-to-AFM phase transition occurs around 30 K in $Er_5Si_3B_x$ compounds. However, the magnetic behavior of $Er_5Si_3B_x$ compounds at temperatures below 30 K is still unclear and therefore the $M(T)$ curves under different magnetic fields are shown in Figs. 2(c) and 2(d). It can be clearly observed that a typical field-induced metamagnetic transition from the AFM state to the FM state occurs around 10 K and 30 K for $Er_5Si_3B_x$ compounds as the magnetic field increases. The results show that the strengths of the exchange interaction between the two AFM states around 10 K and 30 K are different, based on the critical magnetic field required for field-induced metamagnetic transition from the AFM to the FM state. The AFM state

around 10 K requires a magnetic field higher than that at least 4 T to undergo the field-induced metamagnetic transition from AFM to FM, while the antiferromagnetic state around 30 K undergoes a similar transition at an applied magnetic field of more than 1.8 T. However, the magnetic structure in the temperature range 10–30 K is still complicated as a result of the competition between the low-temperature AFM I ($\sim$ 10 K) and the high-temperature AFM Ⅱ ($\sim$ 30 K), with magnetic interactions similar to those of ferrimagnetic state (FiM). In the PM region, the inverse dc susceptibility ($1/\chi$) follows the Curie–Weiss law as shown in Figs. 2(a) and 2(b) insets. The $1/\chi$–T curves are based on the Curie–Weuss fits to PM Curie temperatures (θ_{CW}) of 18.7 K and 17.9 K in $Er_5Si_3B_x$ compounds. The positive θ_{CW} indicates that the AFM interaction in $Er_5Si_3B_x$ compounds is unstable, and similar phenomena have been observed in other AFM compounds as well.[37,38]

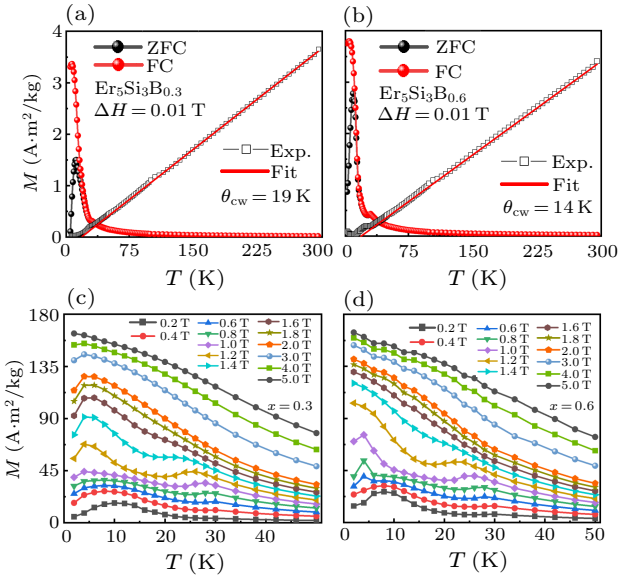


Fig. 2. $M(T)$ of $Er_5Si_3B_x$ ($x = 0.3$, 0.6) compounds [(a), (b)] under 0.01 T and [(c), (d)] under different magnetic fields.

The isothermal magnetization $M(H)$ curves of $Er_5Si_3B_x$ compounds were measured to further understand their magnetic and magnetic phase transitions, the curves for different temperatures can be observed in Figs. 3(a)–3(d). It can be clearly seen that M of $Er_5Si_3B_x$ compounds first rises sharply at 2 K and then shows a linear increase, M again increases sharply with further increase in the magnetic field and gradually tends to saturation. The same phenomenon can be observed in the EuSe compound, which may be due to the successive magnetic phase transitions from AFM I to FiM, then to AFM Ⅱ.[39,40] In addition, the $M(H)$ curves exhibit a clear crossover around 10 K and 30 K, which is caused by AFM interactions. In the PM temperature region (temperatures above 30 K), M increases linearly with increasing magnetic field, which is consistent with the results obtained above. It is well known that there is a close correlation between the MCE and the type of magnetic phase transition. Thus, the $M(H)$ curves with increasing and decreasing magnetic field for different temperatures are shown in Figs. 3(a) and 3(b). The results show that there is significant hysteresis in $Er_5Si_3B_x$ compounds at 2 K, which is due to the transition from AFM I to FiM. As the temperature increases, only a slight hysteresis exists at 10 K. Remarkably, the hysteresis disappears almost completely at 20 K, indicating that the magnetic phase transition from FiM to AFM Ⅱ is reversible. Based on the Banerjee criterion the Arrott plots indirectly obtained from the $M(H)$ curve was applied to further determine the order type of magnetic transitions of $Er_5Si_3B_x$ compounds.[41] The order of the magnetic phase transition is determined by the negative or positive slope of the curve of the Arrott plots corresponding to the first and second order phase transitions, respectively. As the temperature is below 30 K, the Arrott polts exhibits a distinct S-shape, indicating the presence of both first- (AFM I to FiM) and second-order (AFM Ⅱ to FiM) magnetic phase transitions in $Er_5Si_3B_x$ compounds as shown in Figs. 4(c) and 4(d).

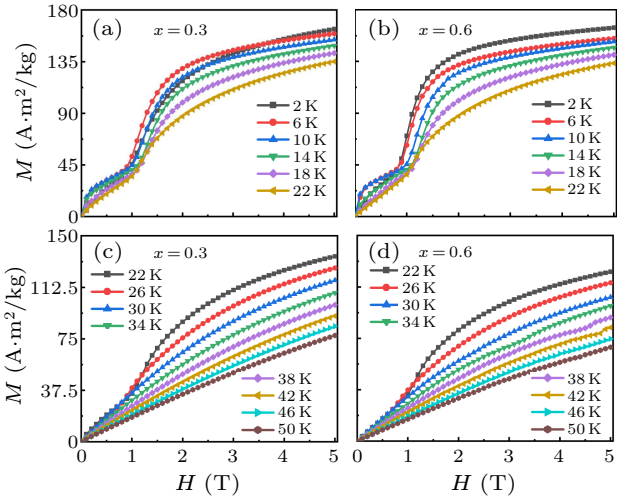


Fig. 3. $M(H)$ curves of $Er_5Si_3B_x$ ($x = 0.3$, 0.6) compounds: [(a), (b)] $T = 2$–22 K, [(c), (d)] $T = 38$–50 K. [(a), (c)] $x = 0.3$, [(b), (d)] $x = 0.6$.

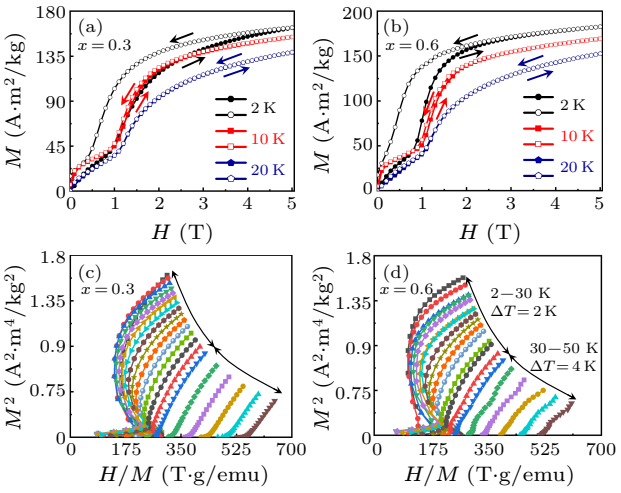


Fig. 4. [(a), (b)] $M(H)$ curve with increasing and decreasing magnetic field, and [(c), (d)] the Arrott plot (H/M vs. M^2), for $Er_5Si_3B_x$ ($x = 0.3$, 0.6).

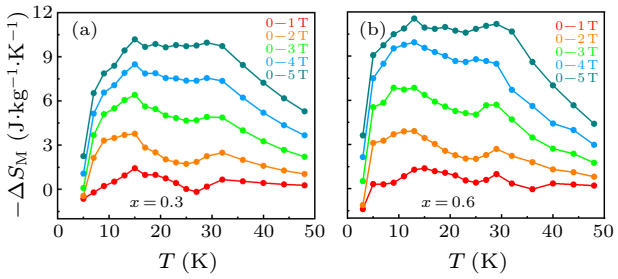


Fig. 5. $\Delta S_{\rm M}(T)$ curves of $Er_5Si_3B_x$ ($x = 0.3$, 0.6) compounds.

The magnetic entropy change $S_{\rm M}(T,\Delta H)$ for $Er_5Si_3B_x$ compounds have been determined based on the Maxwell thermodynamic relation for the variation of the magnetic field in the range 0–5 T, the corresponding results are shown in Figs. 5(a) and 5(b).[42]

$$\Delta S_{\rm M}(T,H) = S_{\rm M}(T,H) - S_{\rm M}(T,0) = \int_0^H \left(\frac{\partial M(T,H)}{\partial T}\right)_H {\rm d}H. \quad (1)$$

As the magnetic field varies in the range 0–1 T, there is a significant negative value of $-\Delta S_{\rm M}$ that is caused by AFM interactions. However, owing to the successive complex magnetic phase transitions in $Er_5Si_3B_x$ compounds the $-\Delta S_{\rm M}$ exhibits approximately constant values under varying magnetic fields at 0–5 T and the corresponding values of $-\Delta S_{\rm M}^{\rm max}$ are 10.2 J·kg^{-1}·K^{-1} and 11.5 J·kg^{-1}·K^{-1}. To further evaluate the magnetothermal effects of $Er_5Si_3B_x$ compounds, RC [Eq. (2)] and TEC [Eq. (3)] can be determined by[43,44]

$${\rm RC} = \int_{T_{\rm cold}}^{T_{\rm hot}} |S_{\rm M}(T)|\,{\rm d}T, \quad (2)$$

$${\rm TEC} = \frac{1}{\Delta T_{\rm lift}} \left\{ \int_{T_{\rm mid}-\frac{\Delta T_{\rm lift}}{2}}^{T_{\rm mid}+\frac{\Delta T_{\rm lift}}{2}} \Delta S_{\rm M}(T)_{\Delta H,T}\,{\rm d}T \right\}, \quad (3)$$

where $T_{\rm hot}$ and $T_{\rm cold}$ are the temperatures corresponding to the values of $\frac{1}{2}|-\Delta S_{\rm M}^{\rm max}|$, respectively. TEC is the average value of $-\Delta S_{\rm M}$ over a defined temperature range. $T_{\rm mid}$ is the temperature of the maximum TEC ($\Delta T_{\rm lift}$) that can be obtained over a specific temperature region and the $\Delta T_{\rm lift}$ is the desired range of temperature to be obtained. The RCs for $Er_5Si_3B_x$ compounds under varying magnetic fields from 0 to 5 T are 356.38 J/kg and 393.37 J/kg. Remarkably, owing to the $-\Delta S_{\rm M}^{\rm max}$ in the proximity of the magnetic phase transition, the successive magnetic phase transitions in $Er_5Si_3B_x$ compounds lead to a wide temperature range for $-\Delta S_{\rm M}^{\rm max}$, corresponding to TEC (30) of 9.33 J·kg^{-1}·K^{-1} and 10.65 J·kg^{-1}·K^{-1}, respectively, under varying magnetic fields from 0 to 5 T. Compared to the $-\Delta S_{\rm M}^{\rm max}$, the TEC (30) is only 9% lower, which is unique among all magnetic refrigeration materials. Therefore, the $Er_5Si_3B_x$ compounds are ideal magnetic refrigeration materials for applications in Ericsson cycle-based magnetic refrigeration systems.

4. Conclusions

In summary, we have synthesized polycrystalline $Er_5Si_3B_x$ ($x = 0.3$, 0.6) compounds and investigated their structure, magnetic properties, magnetic phase transitions and MCEs. The lattice constant change caused by the doping of element B affects the orbital exchange interactions for Er^{3+} ions, which leads to the interesting and complex magnetic properties observed in the $Er_5Si_3B_x$ ($x = 0.3$, 0.6) compounds. In addition, the field-induced metamagnetic transitions are observed with increasing magnetic fields. The $-\Delta S_{\rm M}^{\rm max}$ and RC of $Er_5Si_3B_x$ ($x = 0.3$, 0.6) compounds are 10.2 J·kg^{-1}·K^{-1}, 356.3 J·kg^{-1}·K^{-1} and 11.5 J·kg^{-1}·K^{-1}, 393.3 J·kg^{-1}·K^{-1} under varying magnetic fields from 0 to 5 T. The successive magnetic phase transitions cause the $-\Delta S_{\rm M}$ to be nearly constant over a wide temperature range, with corresponding TEC (30) of 9.3 J·kg^{-1}·K^{-1} and 10.6 J·kg^{-1}·K^{-1}. Our results show that $Er_5Si_3B_x$ ($x = 0.3$, 0.6) compounds are optimally suitable magnetic refrigeration materials for application in Ericsson cycle-based magnetic refrigerators.

Acknowledgment

This work was supported by Science and Technology Research Project for Education Department of Jiangxi Province, China (Grant No. GJJ218509).

References

[1] Cheng W, Ding D and Lei X 2016 *Chin. Phys. Lett.* **33** 16102
[2] Hu F, Zhang G Y, Huang Y J, *et al.* 2014 *Chin. Phys. Lett.* **31** 057501
[3] Yu X Y, Feng H L, Gu X, *et al.* 2019 *Acta Phys. Sin.* **68** 247201 (in Chinese)
[4] Li G Q, Ke Y J, Zhang H B, *et al.* 2019 *Acta Phys. Sin.* **68** 217501 (in Chinese)
[5] Cao Y Z and Zhao Y 2019 *Acta Phys. Sin.* **68** 168502 (in Chinese)
[6] Chen X and Zhang M H 2018 *Acta Phys. Sin.* **67** 197501 (in Chinese)
[7] Tang B Z, Liu X P, Li D M, Yu P and Xia L 2020 *Chin. Phys. B* **29** 056401
[8] Ma Y F, Tang B Z, Xia L and Ding D 2016 *Chin. Phys. B* **33** 126101
[9] Bao L F, Huang W D and Ren Y J 2016 *Chin. Phys. Lett.* **33** 77502
[10] Tian L, Gong J J, Fu Q, Gao X Q, Mo Z J, Li Z X and Shen J 2023 *J. Magn. Magn. Mater.* **566** 170194
[11] Tian L, Fu Q, Mo Z J, Sun H, Li Z X, Shen J and Liu G D 2023 *J. Magn. Magn. Mater.* **576** 170770
[12] Cheng J H, Wang Y G and Xie D 2015 *Chin. Phys. Lett.* **32** 17503
[13] Ding D, Zhang Y Q and Xia L 2015 *Chin. Phys. Lett.* **32** 106101
[14] Mo Z J, Shen J, Yan L Q, Tang C C, Lin J, Wu J F, Sun J R, Wang L C, Zheng X Q and Shen B G 2013 *Appl. Phys. Lett.* **103** 052409
[15] Ding D, Wang P, Guan Q, *et al.* 2013 *Chin. Phys. Lett.* **30** 096104
[16] Hao Z H, Wang H Y, Zhang Q, *et al.* 2018 *Acta Phys. Sin.* **67** 247502 (in Chinese)
[17] Zhang H, Xing C F, Long K W, *et al.* 2018 *Acta Phys. Sin.* **67** 207501 (in Chinese)
[18] Yang J J, Zhao J L, Xu L, *et al.* 2018 *Acta Phys. Sin.* **67** 077501 (in Chinese)
[19] Guo D, Zhang Y K, Wang Y M, *et al.* 2020 *Chin. Phys. B* **29** 107502
[20] Ding Y H, Meng F Z and Wang L C 2020 *Chin. Phys. B* **29** 077501
[21] Hao J Z, Hu F X, Yu Z B, *et al.* 2020 *Chin. Phys. B* **29** 047504
[22] Liu P F, Peng J, Xue M Q, *et al.* 2020 *Chin. Phys. B* **29** 047503
[23] Jiang W H, Mo Z J and Luo J W 2020 *Chin. Phys. B* **29** 037502
[24] Yu T L, Yu X Y, Yang E, *et al.* 2019 *Chin. Phys. B* **28** 067501

[25] Yao G Q, Sun S Y, Yang J C, Wu H F, Wang Q, Zhu J and Cui W B 2021 *Scr. Mater.* **194** 113649

[26] Takeya H, Pecharsky V K, Gschneidner K A and Moorman J O 1994 *Appl. Phys. Lett.* **64** 2739

[27] Zhang Y K, Xu P, Zhu J, Yan S M, Zhang J C and Li L W 2023 *Mater. Today Phys.* **32** 101031

[28] Sun H, Wang J F, Tian L, Gong J J, Mo Z J, Shen J and Shen B G 2022 *Chin. Phys. B* **31** 117503

[29] Zhang Y K, Guo D, Li H D, Geng S H, Wang J, Li X, Xu H, Ren Z M and Wilde G 2018 *J. Alloys Compd.* **733** 40

[30] Feng J Q, Liu Y H, Sui J H, He A N, Xia W X, Wang W H and Wang J Q 2021 *Mater. Today Phys.* **21** 100528

[31] Li L W, Yuan Y, Qi Y, Wang Q and Zhou S Q 2017 *Mater. Res. Lett.* **6** 67

[32] Balfour E A, Shang Y F, Zheng Q, Cao Y T, Fu H, E-Gendy A A and Hadimani R L 2018 *J. Magn. Magn. Mater.* **467** 108

[33] Zhang H, Xu Z Y, Zheng X Q, Shen J, Hu F X, Sun J R and Shen B G 2012 *Solid State Commun.* **152** 1127

[34] Semitelou I P, Yakinthos J K and Roudaut E 1995 *J. Phys. Chem. Solids* **56** 891

[35] Roger J, Yahia M B, Babizhetskyy V, Bauer J, Cordier S, Guerin R, Hiebl K, Rocquefelte X, Saillard J Y and Halet J F 2006 *J. Solid State Chem.* **179** 2310

[36] Mohapatra N, Mukherjee K, Iyer K K and Sampathkumaran E V 2011 *J. Phys.: Condens. Matter* **23** 496001

[37] Zhang H, Wu Y Y, Long Y, Wang H S, Zhong K X, Hu F X, Sun J R and Shen B G 2014 *J. Appl. Phys.* **116** 213902

[38] Hermes W, Rodewakd U C and Pottgen R J *Appl. Phys.* **108** 113919

[39] Li D X, Yamamura T, Nimori S, Homma Y and Honda F 2013 *Appl. Phys. Lett.* **102** 152409

[40] Fukuma H, Suzuki T and Kasuya T 1985 *J. Magn. Magn. Mater.* **52** 7

[41] Banerjee B K 1964 *Phys. Lett.* **12** 16

[42] Franco V, Blázquez J S and Upus J J 2018 *Prog. Mater. Sci.* **93** 112

[43] Gschneidner K A and Pecharsky V K 2000 *Annu. Rev. Mater. Sci.* **30** 387

[44] Griffith L D, Mudryk Y, Slaughter J and Pecharsky V K J *Appl. Phys.* **123** 034902